



HAL
open science

Tuning spin filtering by anchoring groups in benzene derivative molecular junctions

Dongzhe Li, Yannick J Dappe, Alexander Smogunov

► **To cite this version:**

Dongzhe Li, Yannick J Dappe, Alexander Smogunov. Tuning spin filtering by anchoring groups in benzene derivative molecular junctions. *Journal of Physics: Condensed Matter*, 2019, 31 (40), pp.405301. 10.1088/1361-648X/ab2846 . hal-02336477

HAL Id: hal-02336477

<https://hal.science/hal-02336477>

Submitted on 30 Oct 2019

HAL is a multi-disciplinary open access archive for the deposit and dissemination of scientific research documents, whether they are published or not. The documents may come from teaching and research institutions in France or abroad, or from public or private research centers.

L'archive ouverte pluridisciplinaire **HAL**, est destinée au dépôt et à la diffusion de documents scientifiques de niveau recherche, publiés ou non, émanant des établissements d'enseignement et de recherche français ou étrangers, des laboratoires publics ou privés.

Tuning spin filtering by anchoring groups in benzene derivative molecular junctions

Dongzhe Li

Department of Physics, University of Konstanz, 78457 Konstanz, Germany

E-mail: dongzhe.li@uni-konstanz.de

Yannick J. Dappe

Service de Physique de l'Etat Condensé (SPEC), CEA, CNRS, Université Paris-Saclay, CEA Saclay 91191 Gif-sur-Yvette Cedex, France

Alexander Smogunov

Service de Physique de l'Etat Condensé (SPEC), CEA, CNRS, Université Paris-Saclay, CEA Saclay 91191 Gif-sur-Yvette Cedex, France

Abstract. One of important issues of molecular spintronics is the control and manipulation of charge transport and, in particular, its spin polarization through single-molecule junctions. Using *ab initio* calculations, we explore spin-polarized electron transport across single benzene derivatives attached with six different anchoring groups (S, CH₃S, COOH, CNH₂NH, NC and NO₂) to Ni(111) electrodes. We find that molecule-electrode coupling, conductance and spin polarization (SP) of electric current can be modified significantly by anchoring groups. In particular, a high spin polarization (SP > 80%) and a giant magnetoresistance (MR > 140%) can be achieved for NO₂ terminations and, more interestingly, SP can be further enhanced (up to 90%) by a small voltage. The S and CH₃S systems, on the contrary, exhibit rather low SP while intermediate values are found for COOH and CNH₂NH groups. The results are analyzed in detail and explained by orbital symmetry arguments, hybridization and spatial localization of frontier molecular orbitals. We hope that our comparative and systematic studies will provide a valuable quantitative information for future experimental measurements on that kind of systems and will be useful for designing high-performance spintronics devices.

Keywords: Molecular spintronics, NEGF-DFT calculations, Spin filtering, Single-molecule junctions

1. Introduction

Molecular (organic) spintronics [1] is a rapidly developing field of research, aiming at the manipulation of both electron charge and spin in molecular-based devices, taking advantage of large spin relaxation length across purely organic molecules due to small spin-orbit interactions. The one of most fundamental and crucial properties here is the

24 spin polarization (SP) of the current by ferromagnet/organic interface [2, 3, 4], which
 25 can be defined as $SP = (G_{\downarrow} - G_{\uparrow}) / (G_{\uparrow} + G_{\downarrow}) \times 100\%$, where G_{\uparrow} and G_{\downarrow} are spin up
 26 (majority) and spin down (minority) conductance, respectively. Recently, it has been
 27 shown that the SP in single molecule junctions can be tuned by a mechanical strain [5],
 28 an orbital symmetry considerations [6], and spin-dependent quantum interference effect
 29 [7] etc. Understanding physical and chemical mechanisms involved in spin injection at
 30 the hybrid interfaces for further design of possible molecular-based devices with large
 31 SP and high conductance is one of the most important issues in this field.

32 The anchoring groups (also known as “linkers”) placed at extremities of the
 33 molecule are responsible for establishing a stable mechanical contact and efficient
 34 molecule/metal electronic coupling. For this reason, thiol ($-\text{SH}$) [8] and thiolate ($-\text{S}$)
 35 [9, 10] have become the most widely used anchoring groups due to strong covalent
 36 gold-sulfur bonding. However, it was argued extensively that the conductance of thiol
 37 based molecular junctions depends strongly on the binding geometry [11]. Therefore,
 38 many theoretical and experimental efforts were made to explore various anchoring groups
 39 such as methylthiol ($-\text{CH}_3\text{S}$) [12, 13], carboxyl-acids ($-\text{COOH}$) [8, 14], amidine ($-\text{NH}_2$)
 40 [10, 15], isonitrile ($-\text{NC}$) [16, 17], nitrile ($-\text{N}$) [18], nitro ($-\text{NO}_2$) [19, 20], etc. These
 41 investigations ended up with two general conclusions : first, the chemical nature of
 42 anchoring groups strongly affects the energy level alignment of molecular frontier orbitals
 43 with respect to the metal Fermi level; second, the degree of hybridization between
 44 molecule and metal changes dramatically with anchoring groups.

45 For $3d$ ferromagnetic materials, the s band is almost non spin-polarized while the $3d$
 46 bands are spin-split due to the exchange interactions. As a result, the density of states
 47 (DOS) of $3d$ ferromagnetic materials (such as Fe, Co, or Ni) show a spin polarization of
 48 about 30~40% at the Fermi energy. Therefore, when organic molecules are contacted
 49 with $3d$ metals, a selective hybridization occurs at the molecule-metal interface for
 50 spin up and down channels. For example, due to large $\pi - d$ hybridization at the
 51 ferromagnetic metal/organic interfaces, high spin polarization [2, 21], controllable ferro-
 52 or antiferromagnetic interlayer exchange coupling [22], giant magnetoresistance [23] and
 53 enhanced perpendicular magnetic anisotropy [24] were reported (a detailed discussion
 54 on molecular spinterface can be found in Ref. [25]).

55 Previous studies were mainly focused on the effect of anchoring groups on
 56 charge transport properties with nonmagnetic electrodes (Au, Ag and Cu etc). The
 57 investigation of spin polarization via various anchoring groups at organic spinterface was
 58 pointed out recently [26, 27]. In this work, based on spin-polarized *ab initio* transport
 59 calculations, we present a comparative and systematic study of the impact of anchoring
 60 groups on spin-dependent transport with ferromagnetic electrodes. More specifically, we
 61 have chosen a benzene as a core structure and have studied the spin-dependent transport
 62 for a series of $\text{Ni}(111)/\text{X}-(\text{C}_6\text{H}_4)-\text{Y}/\text{Ni}(111)$ junctions, where terminations X,Y could
 63 be S, CH_3S , COOH , CNH_2NH , NC or NO_2 groups, as demonstrated in Fig. 1. These
 64 systems are chosen because Ni-based spin valves were firstly proposed by Emberly *et al*
 65 [28] as a prototypical molecular spintronic system, and later on were studied extensively

66 by several theory groups based on *ab initio* methods [29, 30] and also successfully created
 67 by mechanically controlled break junction (MCBJ) experiment [31]. Importantly, as will
 68 be discussed later, all these molecules have frontier orbitals which, by symmetry, do not
 69 overlap with the Ni electrode’s *s* states. Due to symmetry arguments proposed by us
 70 recently [6, 32], all the junctions are therefore expected to display rather high SP of
 71 conductance which is indeed confirmed by our calculations. We find, moreover, that
 72 among all considered molecules the one with NO₂ terminations, M6 in Fig. 1, presents
 73 very high values of SP and of total conductance at the same time. In addition, high spin
 74 filtering in M6 (–NO₂) is accompanied by huge magnetoresistance (MR) ratio (about
 75 140%) which measures the change in resistance (or conductance) between parallel and
 76 antiparallel magnetic configurations of two ferromagnetic electrodes. These findings
 77 make therefore M6 molecule the most promising candidate for possible spintronics
 78 applications.

79 The paper is organized as follows. In Sec. 2, we present computational methods and
 80 models used in this work. In Sec. 3, the electronic structure and transport properties
 81 of benzene derivative molecules with different anchoring groups in equilibrium will be
 82 presented. Then, we will present the non-equilibrium transport phenomena with a
 83 particular focus on their SP and MR. Finally, the conclusion will be drawn in Sec. 4.

84 2. Calculation methods and models

85 The geometry optimization of molecular junctions was carried out using plane waves
 86 QUANTUM-ESPRESSO (QE) package [33] within the density functional theory (DFT).
 87 We used PBE [34] exchange-correlation functionals and ultrasoft pseudopotentials (PP)
 88 to describe electron-ion interactions. Plane-wave energy cutoffs of 30 and 300 Ry were
 89 used for wave functions and charge density, respectively. Molecular junctions were
 90 described in a supercell containing a molecule and two 4-atom Ni pyramids attached
 91 to both sides to Ni(111) slabs with 4×4 periodicity in the *XY* plane (16 atoms per
 92 layer) containing 6 layers on each side as shown in Fig. 1. During ionic relaxation, three
 93 bottom layers on both sides were kept fixed at their bulk positions while a molecule and
 94 other Ni layers were allowed to relax until atomic forces were less than 10^{-3} Ry/Bohr.
 95 Relaxation was performed using $(2 \times 2 \times 1)$ *k*-point mesh.

96 After the atomic relaxation, *ab initio* spin-polarized electronic transport properties
 97 for different molecular junctions were evaluated using the TRANSIESTA code [35] which
 98 employs a non-equilibrium Green’s function (NEGF) formalism combined with DFT.
 99 We used Troullier-Martins norm-conserving pseudopotentials [36], PBE functional and
 100 an energy cutoff for the real-space mesh of 250 Ry. Valence electron wavefunctions were
 101 expanded in a basis of local orbitals in SIESTA [37]. A double ζ plus polarization (DZP)
 102 basis set with an energy shift of 50 meV was used, which resulted, as we have checked, in
 103 a good agreement with QE results for both magnetic properties and energy alignments
 104 (see Fig. 6 in Appendix A). The convergence tolerance for self-consistent loop was set
 105 to 10^{-4} eV and the Brillouin zone was sampled by $6 \times 6 \times 1$ *k*-point mesh.

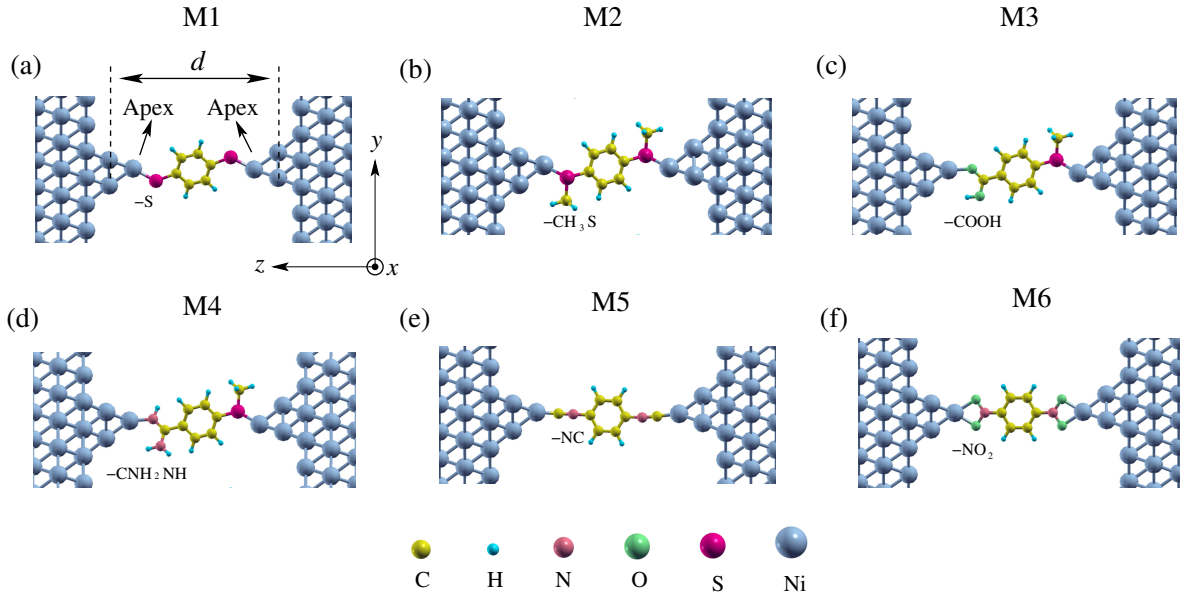


Figure 1. Schematic representation of optimized atomic structures for benzene-based molecules with different anchoring groups connecting two Ni(111) electrodes. The investigated six molecules in this work are: (a) 1,4-benzenedithiolate (M1), (b) benzene, 1,4-bis (methylthio) (M2), (c) 4-(methylthio) benzoic acid (M3), (d) benzene, 1,4-amine and methylthio (M4), (e) 1,4-phenylene diisocyanide (M5) and (f) 1,4-dinitrobenzene (M6). Note that M3 and M4 are asymmetric molecular junctions with different anchoring groups on the left and right sides. Z is the charge transport direction which is parallel to the junction axis.

	d (Å)	$d_{\text{Ni-X}}$ (Å)	$d_{\text{Ni-Y}}$ (Å)	M_s (μ_B)	G_{\uparrow} ($G_0 = e^2/h$)	G_{\downarrow} ($G_0 = e^2/h$)	G_{tot} ($G_0 = e^2/h$)	SP (%)
M1	13.78	2.14	2.14	0.28	1.48×10^{-1}	7.15×10^{-2}	2.20×10^{-1}	-34.99
M2	13.45	2.16	2.16	-0.02	9.81×10^{-3}	7.77×10^{-3}	1.76×10^{-2}	-11.50
M3	14.03	2.11	1.89	-0.07	1.73×10^{-2}	8.80×10^{-2}	9.77×10^{-2}	64.49
M4	14.24	2.12	1.89	-0.04	1.51×10^{-2}	4.10×10^{-2}	5.62×10^{-2}	46.00
M5	15.25	1.78	1.78	-0.14	1.67×10^{-2}	2.78×10^{-1}	2.50×10^{-1}	87.46
M6	14.24	2.04	2.04	0.31	3.54×10^{-2}	3.21×10^{-1}	3.56×10^{-1}	80.13

Table 1. Optimized junction distances, induced molecular spin moment (M_s) (calculated from spin-polarized molecular DOS integrated up to the Fermi energy as shown in Fig. 7), spin-resolved and total conductances (in the unit of $G_0 = e^2/h$ which is conductance quantum per spin) in parallel spin configuration and its spin polarization.

106 Spin-resolved (denoted by spin index $\sigma = \uparrow, \downarrow$) transmission function, depending on
 107 energy E and applied bias V_b , is given by:

$$T_{\sigma} = \text{Tr}[\Gamma_{L,\sigma} G_{\sigma}^r \Gamma_{R,\sigma} G_{\sigma}^a], \quad (1)$$

108 where all matrices depend also on E and V_b and have dimension of the scattering
 109 region (or extended molecule) including the molecule itself and some parts of left and
 110 right electrodes (where screening takes place). $G_{\sigma}^{r/a}$ are the retarded/advanced Green's
 111 functions:

$$G_\sigma^{r/a} = [(E \pm i\eta)S - H_\sigma^C - \Sigma_{L,\sigma}^{r/a} - \Sigma_{R,\sigma}^{r/a}]^{-1} \quad (2)$$

with η is an infinitesimal positive number, S is the overlap matrix, H_σ^C is the Hamiltonian matrix for the scattering region and $\Sigma_{L/R,\sigma}^{r/a}$ are retarded or advanced self-energies due to left/right electrodes. Coupling matrices $\Gamma_{L/R,\sigma}$ are evaluated from corresponding self-energies as $\Gamma_{L/R,\sigma} = i(\Sigma_{L/R,\sigma}^r - \Sigma_{L/R,\sigma}^a)$.

Finally, the spin-dependent charge current is obtained from the Landauer-Büttiker formula:

$$I_\sigma(V_b) = \frac{e}{h} \int_{-\infty}^{+\infty} dE [f(E, \mu_L) - f(E, \mu_R)] T_\sigma(E, V_b), \quad (3)$$

where $f(E, \mu_{L/R})$ are Fermi-Dirac distribution functions, and $\mu_{L/R}$ are electrochemical potential of left/right electrodes.

3. Results and discussion

The optimized geometries of molecular junctions are shown in Fig. 1. We first performed atomic relaxations of a Ni/molecule interface to obtain an electrode-molecule separation and geometry, and then carried out full relaxations by attaching the second electrode at the previously calculated molecule-metal distance. Let us stress that relaxations have been performed starting from several possible initial configurations in order to find the minimum energy configuration. For example, the nitro ($-\text{NO}_2$)-terminated molecule prefers to bind through double Ni–O bonds on each side rather than with Ni–N or single Ni–O bonds as seen in Fig. 1 (f). Some important structural parameters, electronic and transport properties are summarized in Table 1. Note that M3 and M4 are asymmetric junctions with two different linking groups on left and right sides while all the others are symmetric. Small induced (by Ni electrodes) spin moments on M1 and M6 were found to be positive (“ferromagnetic” molecule/Ni coupling) while for other molecules – negative (“antiferromagnetic” coupling). Spin-dependent conductance, G_σ , is given by the Landauer-Büttiker formula, $G_\sigma = G_0 T_\sigma(E_F)$, where $G_0 = e^2/h$ is the quantum conductance per spin (e being the electron charge and h Planck’s constant) and $T_\sigma(E_F)$ is the transmission function for spin $\sigma = \uparrow, \downarrow$ at the Fermi energy. The calculated total conductance (summed over spin up and down channels) of M1 at zero bias voltage was found to be about $0.22G_0$ which is in agreement with previous calculations [38]. Additionally, the SP of M1 and M2 was found to be negative ($G_\uparrow > G_\downarrow$) while all the junctions have positive SP. Previous DFT calculations showed also a negative SP in Ni/BDT/Ni junction [29]. Moreover, M5 and M6 exhibit large spin polarization of about 87% and 80% and high conductance of about $0.25G_0$ and $0.35G_0$, respectively, so they appear to be most attractive for possible future applications in spintronics devices.

First, we plot in Fig. 2 highest occupied molecular orbitals (HOMO) as well as lowest unoccupied molecular orbitals (LUMO) for all the molecules in gas phase. We found that all the orbitals are of π -type (odd with respect to the molecular YZ plane)

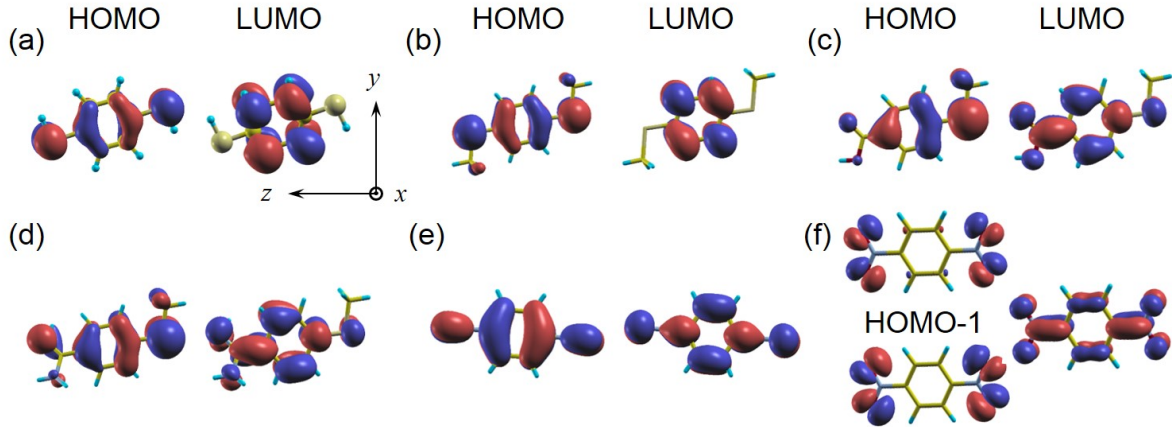


Figure 2. HOMO and LUMO molecular orbitals in gas phase for the same molecules as in Fig.1. Isosurfaces of positive and negative isovalues are shown in red and blue, respectively. Note that all the orbitals are of π -type (odd with respect to the YZ plane) except of HOMO and HOMO-1 for M6 (which are even). The latter orbitals are nearly degenerate (split by about 0.1 eV) and represent bonding/anti-bonding combinations of end-group originated states.

147 except of HOMO and HOMO-1 for M6 case which are split by only about 0.1 eV and
 148 are of σ -type (even with respect to the YZ plane). Interestingly, these M6 orbitals
 149 are both localized on $-\text{NO}_2$ anchoring groups forming a kind of bonding/anti-bonding
 150 states, even or odd with respect to the transport direction Z . Since the molecules have
 151 relatively small tilting angles in the YZ plane, all frontier π -orbitals have rather small
 152 overlap with spin up s -states of Ni apex atoms (two Ni atoms which contact the molecule
 153 as indicated in Fig. 1a) while a strong coupling with spin down d_{xz} states is expected.
 154 That should lead to rather strong SP of conductance due to orbital symmetry argument
 155 [6, 32]. This reasoning is also valid for HOMO and HOMO-1 orbitals of M6, though
 156 they are not of π -type. They are still orthogonal to Ni apex s -states because of odd
 157 symmetry with respect to the XZ plane and will only transmit spin down electrons
 158 injected by Ni apex d_{yz} orbitals.

159 To better understand conductance as well its SP discussed above, we show in Fig.
 160 3 spin-resolved transmission functions at zero bias in the parallel spin configuration of
 161 Ni electrodes. The black and red curves show the spin up and down transmissions,
 162 respectively. First, we note that energy alignment of frontier molecular orbitals with
 163 respect to the Fermi energy, imposed by Ni electrodes, changes drastically with the
 164 anchoring groups. While for M1 and M6 we find that the transport is dominated by the
 165 HOMO (p-type current by holes), in the case of M2, M3, M4 and M5, the conduction
 166 takes place through the LUMO (n-type current by electrons). Second, the width of
 167 transmission features is attributed to the degree of molecule level hybridization with
 168 electrode states. Therefore, much more structured $T(E)$ with broader features is found
 169 for spin down due to extra d_{\downarrow} states of Ni in the vicinity of the E_F . As a general
 170 feature, two peaks are often seen in spin down transmission: the first one at about -0.5

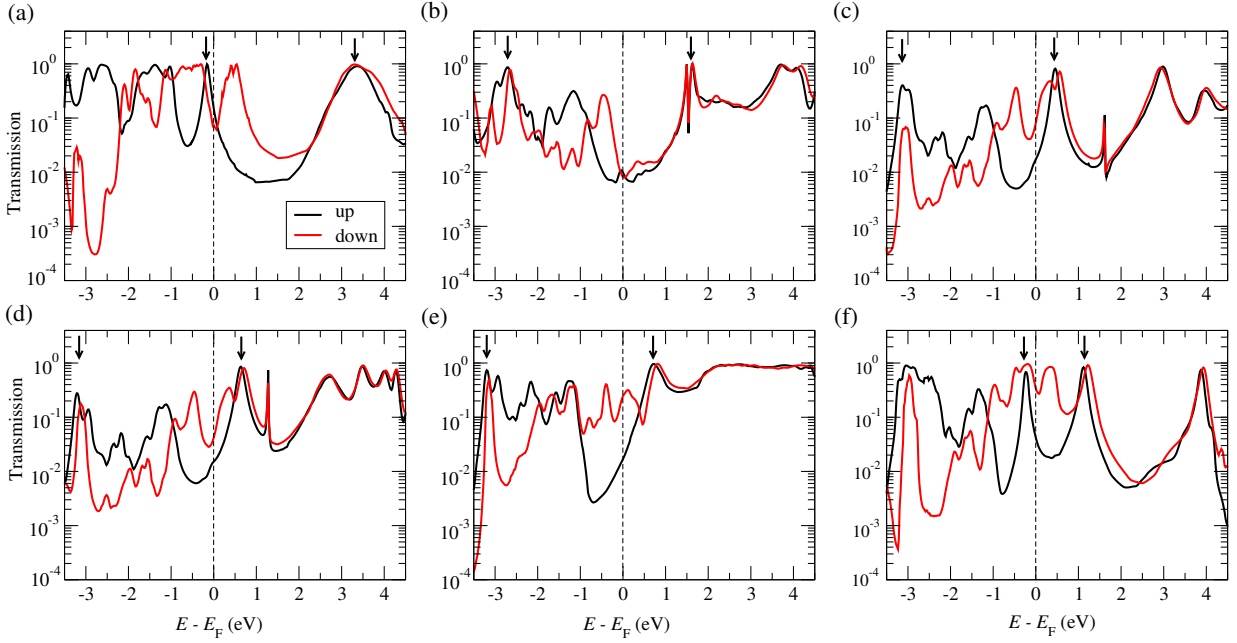


Figure 3. Spin-resolved zero-bias transmission functions (in logarithmic scale) with the parallel magnetic alignment of two Ni electrodes for (a) M1, (b) M2, (c) M3, (d) M4, (e) M5 and (f) M6 molecular junctions. Spin up and down channels are plotted by black and red lines, respectively. Note that the zero of energy is at the Fermi level. Positions of HOMO and LUMO for spin up is marked by black arrow.

171 eV (see, e.g., Fig. 3b-e) and another one at about 0.4 eV (see, e.g., Fig. 3a,c,d,f) which
 172 originate from $d_{x^2-y^2,xy}^\downarrow$ and $d_{zx,zy}^\downarrow$ states, respectively, of Ni apex atoms. Here, we mark
 173 the position of HOMO and LUMO for spin up by black arrow. For the spin down, the
 174 position of HOMO and LUMO are much more delocalized due to strong hybridization
 175 between π orbital and $(s^\downarrow + d^\downarrow)$ states of Ni apexes. For more details, please see the
 176 projected DOS on molecules as shown in Fig. 7 (see Appendix B).

177 We first discuss the electron-donating anchoring groups such as M1 and M6. For
 178 M1, rather sharp spin up peak at about -0.2 eV originates from the HOMO weakly
 179 hybridizing with s_\uparrow states of Ni apexes and with other orbitals of deeper Ni atoms.
 180 For the spin down, much broader feature in transmission is observed at energies -1.2
 181 $\text{eV} < E < 1$ eV coming from the coupling of HOMO with $(s^\downarrow + d^\downarrow)$ states of Ni apexes.
 182 In particular, the peak at about 0.5 eV is related to the offset of Ni d_{xz}^\downarrow states appearing
 183 at about $E < 1$ eV. Another peak in both spin channels at about 3.2 eV is attributed to
 184 the LUMO level. This result is in good agreement with previous *ab initio* calculations
 185 [38, 29]. Interestingly, in the case of M6, compare to M1, the HOMO-derived spin up
 186 transmission peak is more sharp, resulting in significantly reduced spin up conductance
 187 and thus higher spin polarization. This can be explained by two reasons as follows.
 188 The first one is the orbital symmetry argument as mentioned before. During atomic
 189 relaxations, the planar configuration of M1 in the YZ plane is not perfectly conserved, so
 190 it slightly tilts in the X direction and moves out of the YZ plane. This distortion turns

191 out to be much smaller for more symmetric M6 with double Ni–O bonds on both sides.
 192 As a result, the HOMO of M1 is expected to overlap more with Ni apex s -states which
 193 leads to broader spin up transmission peak compared to M6 case. A similar result was
 194 also reported previously in nonmagnetic molecular junctions which can switch between
 195 high and low conductance states by a mechanical strain [39]. The second reason is the
 196 rather strong localization of HOMO and HOMO-1 of M6 on the linking groups (the
 197 orbitals are decoupled in the middle) compared to rather delocalized HOMO of M1 (see
 198 Fig. 2a,f). **By means of stability of molecular junctions with NO₂-termination, we
 199 note that two contradictory results have been reported. L. A. Zotti *et al* [40] concluded
 200 that NO₂-terminated tolanes form rather stable molecular junctions under ambient
 201 conditions with MCBJ while V. Kaliginedi *et al* [41] showed the molecular junctions
 202 formed with NO₂-caped molecule are rather unstable. The authors argued that this
 203 difference may arise from the nature of different experimental conditions in both studies.
 204 Moreover, R. Vardimon *et al* [42] successfully created nickel oxide atomic junctions due
 205 to strong chemisorption at the Ni–O contacts. Therefore, we hope that the M6 (–NO₂)
 206 junction is rather stable with Ni electrodes, and of course this needs to be confirmed by
 207 future experiments.**

208 We now turn our attention to the electron-accepting groups, *i.e.*, M2, M3, M4
 209 and M5. Here, the transport is dominated by LUMO. For M2, when a thiolate
 210 (–S) was replaced by a methylthiol (–CH₃S), the molecule-metal coupling strength
 211 is significantly reduced, resulting in a narrower LUMO resonance peak at about 1.5
 212 eV. Moreover, due to LUMO symmetry (Fig. 2b) it does not overlap with Ni apex
 213 $d_{xz,yz}^{\downarrow}$ states which explains that no increase of spin down transmission is observed
 214 at around 0.4 eV where those d -states dominate the Ni down DOS. That explains
 215 rather low spin down conductance and SP for M2 compared to M1 case. Our results
 216 have a general agreement with very recent experimental measurements on thiolate and
 217 methylthiol terminated systems [43, 44] with Au electrodes. Moreover, in Ref. [44],
 218 the authors confirmed experimentally that S–Au and CH₃S–Au are chemisorption and
 219 physisorption mechanisms, respectively. Next, if we replace one of –CH₃ by –COOH
 220 and –CNH₂NH, forming M3 and M4 asymmetric junctions, the LUMO approaches to
 221 E_F , leading to enhanced conductance. For these molecules, the LUMO (Fig. 2c,d) will
 222 overlap now with $d_{xz,yz}^{\downarrow}$ Ni states so that larger spin down conductance (and noticeable
 223 SP) is again recovered for M3 and M4 junctions which show in fact rather similar
 224 transmission features. **In the case of M3 junction, experimentally, it has been shown
 225 that the formations of –COO[–] and –COOH in solution depend on the pH condition
 226 [8, 14]. Additionally, D. Sheng *et al* used –COOH in their *ab initio* calculations [45]
 227 for alkane molecular wires. The result presented in Fig. 3c, we used COOH–Ni contact
 228 for M3 junction, as shown in Fig. 1c. In addition, we also investigated the M3 junction
 229 with one removed “H” atom forming COO[–]–Ni bond at the interface (see Appendix D).
 230 Interestingly, as shown in Fig. 8, when the “H” atom is removed, the charge transport
 231 is dominated by HOMO rather than LUMO due to loss of one electron. Moreover,
 232 the conductance values for both spins are about one order of magnitude smaller than**

233 corresponding M3 junction because of super sharp HOMO and its localized features
 234 around “O” atoms at the interface (see inset in Fig. 8b). Finally, for M5 molecule
 235 rather broad LUMO-derived transmission feature is seen about 0.75 eV, significantly
 236 increasing for spin down channel upon approaching the Fermi level due to noticeable
 237 coupling to Ni spin down *d*-states. We note that the DFT transport scheme tends to
 238 overestimate the conductance of molecular junctions relative to experiments due to the
 239 underestimation of their gap between occupied and unoccupied states. Quasiparticle
 240 *GW* self-energy has been recognized as a good approximation to describe accurately the
 241 energy level alignment at the molecule-metal interface. However, it has been shown that
 242 *GW* corrections affect rather unoccupied orbitals (poorly described within the ground
 243 state DFT) while occupied levels (in particularly, the HOMO) are only slightly altered
 244 [46, 47]. Since the charge transport in M1 and M6 is dominated by HOMO level, we
 245 hope that the mean-field DFT results are enough to provide reliable comparative results.
 246 On the other hand, for LUMO dominant junctions such as M2, M3, M4 and M5, smaller
 247 conductance values are expected (for both spin channels) with more sophisticated *GW*
 248 self-energy. Moreover, the DFT error is in general systematic, thus conductance ratios
 249 are usually in good agreement with experiment, for instance the rectification ratios
 250 predicted by NEGF-DFT were found to be reliable [48, 49]. So we believe that the spin
 251 filtering ratios presented in this work are reliable as well. In summary, we believe that
 252 the DFT-error introduced here plays a role in a quantitative basis but should not affect
 253 our main conclusions.

254 Having understood the transport properties at equilibrium, we now turn to out-of-
 255 equilibrium situation with a small bias voltage (V_b), up to 0.6 V. At each voltage, the spin
 256 up and down currents are determined self-consistently under non-equilibrium condition
 257 using the Landauer-Büttiker formula (see Eq. 3). The results show various trends for
 258 different anchoring groups. Clearly, spin down current (plotted with negative values) is
 259 significantly larger than the corresponding spin up one (plotted with positive values) as
 260 shown in Fig. 4a. More importantly, for M6, the spin up current increases very slowly
 261 with an approximately linear trend. On the contrary, the spin down current increases
 262 much more rapidly which results in a high spin injection efficiency. The pronounced
 263 increase of spin down currents for M1 and M6 indicates a strong metal/molecule orbital
 264 coupling close to E_F . On the contrary, for M3 and M5, the current for both spin
 265 channels increase much slower. For spin up channel, small currents are attributed to
 266 the fact that the LUMO resonance lie at about 0.5 and 0.7 eV (see Fig. 3) for M3 and
 267 M5, respectively, which are not included in the explored bias window. In addition, we
 268 find that M2 and M4 has lowest currents for both spin channels.

269 The spin polarization of the current at a bias voltage is evaluated as, $SP =$
 270 $(I_\downarrow - I_\uparrow)/(I_\uparrow + I_\downarrow) \times 100\%$, where I_\uparrow and I_\downarrow are spin up and down currents, respectively.
 271 Note that at equilibrium, the SP was evaluated from conductance values. For zero bias
 272 voltage, the SP for M5 and M6 are more than 80%. Interestingly, when the bias voltage
 273 is applied, the SP of M6 is further enhanced up to more than 90%. On the contrary,
 274 the SP of M5 is slightly decreased. Moreover, for M3, the SP is less than 65% under

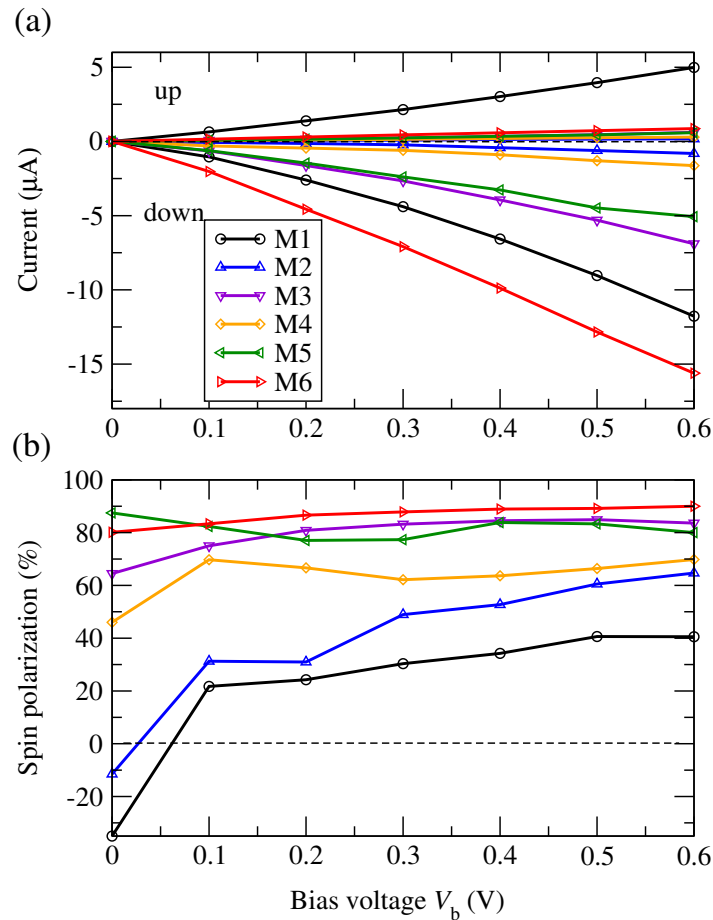


Figure 4. (a) Current-voltage characteristics for spin up (positive values) and spin down (negative values) channel for M1, M2, M3, M4, M5 and M6 molecular junctions, (b) Corresponding SP as a function of voltage. Note that conductance values are used to evaluate SP in equilibrium case.

275 zero bias, but it can become as large as 80% at $V_b = 0.6$ V. On the other hand, the SP
 276 of M4 slightly increases when the bias voltage is applied. Interestingly, the SP of M1
 277 and M2 changes sign when the bias voltage is applied but remains relatively low.

278 Since the M6 exhibits large SP as well as high conductance, we have also studied its
 279 magnetoresistance (MR) property which measures the change in total current between
 280 the parallel (P) and antiparallel (AP) magnetic alignments of Ni electrodes. In the
 281 linear regime it can be calculated as $\text{MR} = (G_P - G_{AP})/G_{AP} \times 100\%$, where G_P
 282 and G_{AP} are total conductances (sum of spin up and down contributions) at zero bias
 283 for P and AP magnetic configurations, respectively. We present in Fig. 5 the total
 284 transmissions for two magnetic cases. As expected, in addition to the large SP the M6
 285 junction also shows very high MR, as large as 140%. It is much larger than the MR
 286 found for M1 junctions, of about 27%, as reported in Ref.[29], confirming once again
 287 very good spin filtering properties of symmetric NO_2 anchoring groups. In appendix D,
 288 we summarized the transmission functions of anti-parallel spin configurations (Fig. 9)

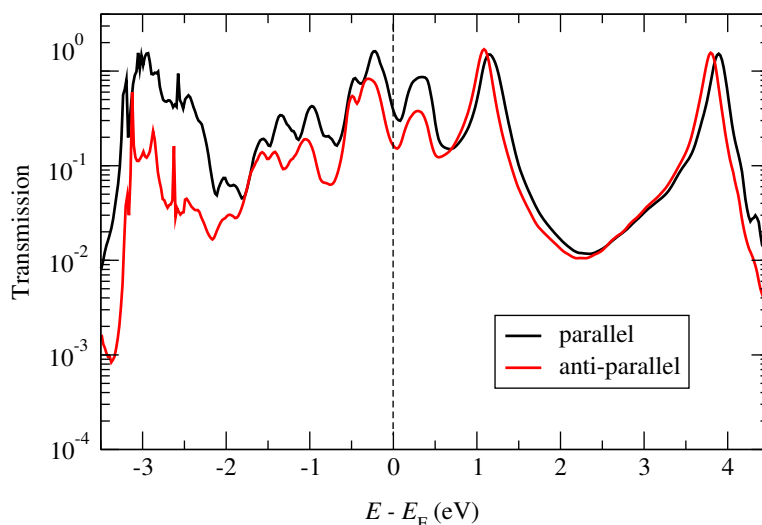


Figure 5. Total transmission functions (in logarithmic scale) of M6 junction at zero-bias voltage for both parallel and anti-parallel magnetic configurations of two Ni electrodes. Note that spin up and down contributions (equal due to symmetry in the antiparallel case) are summed in both configurations. The calculated MR was found to be as large as 140%.

289 and corresponding MR (Table 2) values for all six molecular junctions.

290 4. Conclusions

291 To conclude, by using a combination of density functional theory (DFT) and non-
 292 equilibrium Green's function (NEGF) formalism, we have investigated the effect of
 293 anchoring groups on spin-polarized transport through benzene-derivative molecular
 294 junctions joining two ferromagnetic Ni(111) electrodes. It was found that anchoring
 295 groups have a strong impact on the energy alignment of relevant molecular orbitals with
 296 respect to the Fermi level and the degree of molecule-metal hybridization. Therefore,
 297 the choice of anchoring groups indeed strongly affects the conductance of the molecular
 298 junction and its spin polarization, SP. According to our study, M6 ($-\text{NO}_2$) junctions
 299 exhibit overall the best performance with high conductance (and also the current),
 300 large SP ($>80\%$) as well as giant MR of about 140%. Interestingly, the SP can
 301 be further enhanced (up to 90%) by a small voltage. It was attributed to a rather
 302 sharp/broad HOMO-derived resonance in spin up/down transmission around the Fermi
 303 energy dictated by the HOMO symmetry and its spatial distribution. The S and CH_3S
 304 systems, on the contrary, exhibit rather low SP while intermediate values are found
 305 for COOH and CNH_2NH groups. It has been found, in addition, that the large SP
 306 of M5 ($-\text{NC}$) is slightly decreased with the voltage. We believe that our comparative
 307 and systematic studies will enrich the understanding of the role of anchoring groups on
 308 spin-polarized transport of molecular junctions and will be useful for further studies and
 309 applications in molecular spintronics.

310

 311 **5. Acknowledgments**

 312 D.L. was supported by the Alexander von Humboldt Foundation through a Fellowship
 313 for Postdoctoral Researchers.

314

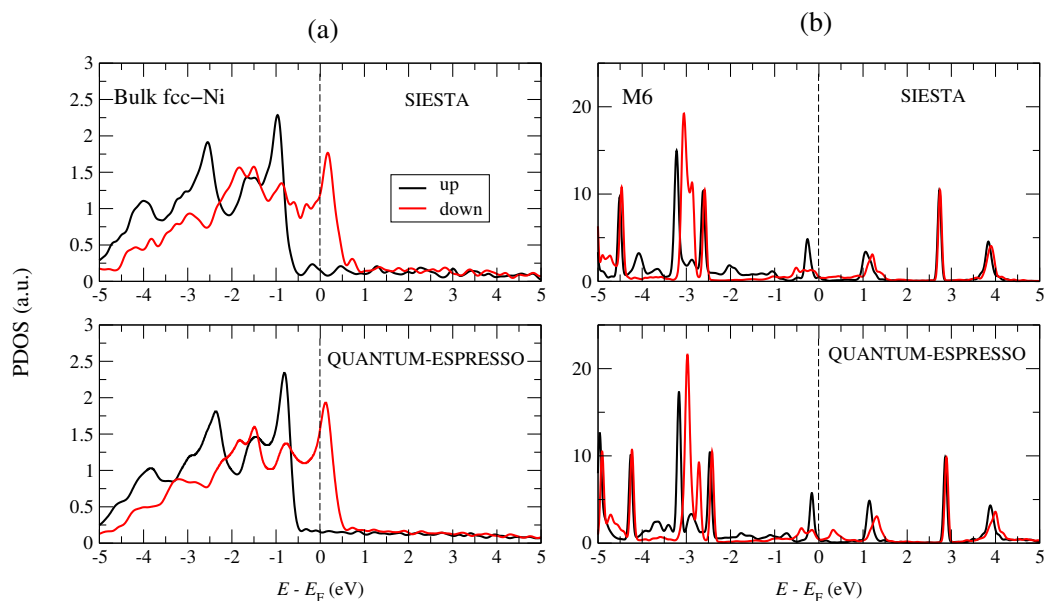
 315 **Appendix A: Comparison between SIESTA and QE results**


Figure 6. (a) Spin-resolved total density of states (DOS) of bulk fcc-Ni for spin up (black) and down (red), calculated by SIESTA (top) with NCPP and by QE with ultrasoft PP (down). The exchange splitting from SIESTA is about 0.16 eV larger, which results in a $0.05 \mu_B$ larger magnetic spin moment compare to QE results. (b) Spin-dependent projected DOS on molecule for M6 junction calculated by SIESTA and QE. A very good overall agreement is found between SIESTA and QE results.

316 For fcc-Ni as seen in Fig. 6 (a), the magnetic moments calculated by QE was
 317 found to be about $0.65 \mu_B$ while the SIESTA within DZP basis gives about $0.70 \mu_B$. The
 318 small discrepancy between QE and SIESTA on spin moment can be traced to the use of
 319 NCPPs in SIESTA, versus ultrasoft PPs in QE. The similar results were also reported in
 320 Ref.[23, 50]. In addition, the single ζ (SZ) and SZP basis sets of SIESTA give the spin
 321 moment of $0.78 \mu_B$ and $0.74 \mu_B$, respectively, suggesting that the DZP basis set for Ni
 322 is the best one in terms of more accurate description of spin moment.

323 In order to check the reliability of our DZP basis sets used in this work, we also
 324 compared the spin-dependent projected DOS on molecule for M6 junctions as plotted in
 325 Fig. 6b. A good agreement between QE and SIESTA results is found in terms of energy
 326 level alignments, indicating the validity of our DZP basis set.

327 **Appendix B: Projected DOS on molecules with the parallel spin**
 328 **configuration**

329 To identify the positions of molecular levels, we display in Fig. 7 the projected DOS
 330 on molecule with the parallel magnetic alignment of two Ni electrodes for six molecular
 331 junctions. HOMO and LUMO peaks are clearly seen.

332 Interestingly, we found that LUMO+1 of M6 (see inset of Fig. 7f) is strongly
 333 localized on 4 carbon atoms of the molecule and is completely decoupled from electrodes,
 334 which explains that no LUMO+1 derived peak was observed in the transmission curve
 335 plotted in Fig. 3 (f).

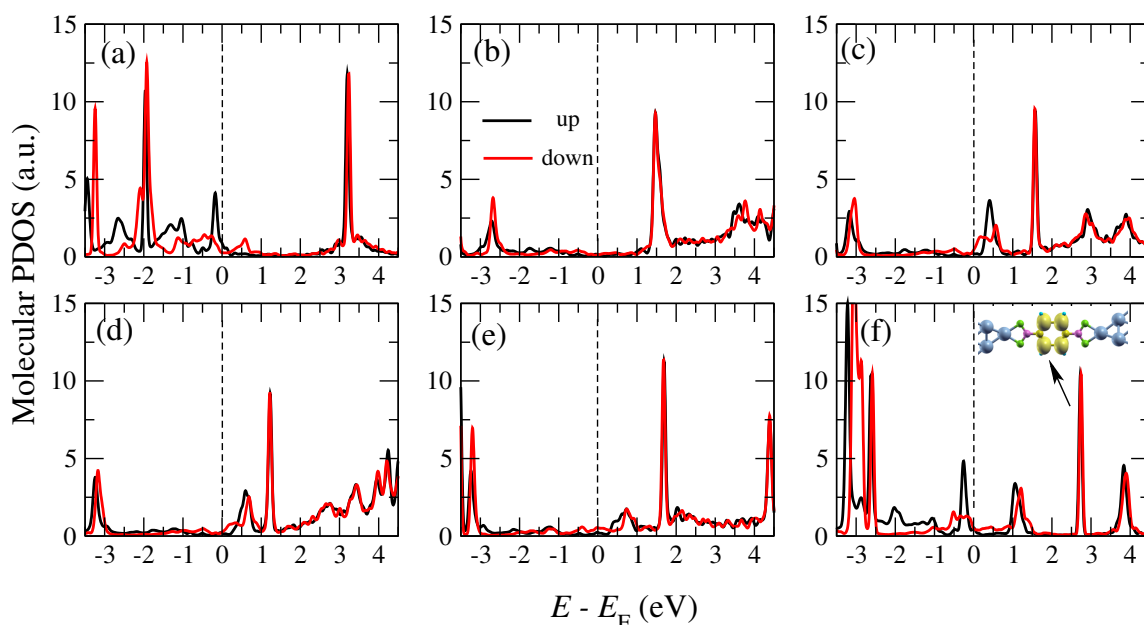


Figure 7. Spin-resolved projected DOS on molecule with the parallel magnetic alignment of two Ni electrodes for (a) M1, (b) M2, (c) M3, (d) M4, (e) M5 and (f) M6 molecular junctions. Spin up and down channels are plotted by black and red lines, respectively. The local DOS in the energy window of LUMO+1 for M6 is also plotted in the inset. Note that the zero of energy is at the Fermi level.

336 **Appendix C: M3 junction with removed single “H”**

337 When the “H” atom is removed, the electron transport is dominated by HOMO rather
 338 than LUMO due to loss of one electron (see Fig. 8). Interestingly, the conductance
 339 values for both spins are about one order of magnitude smaller than corresponding M3
 340 junction because of super sharp HOMO and its localized features around “O” atoms at
 341 the interface (see inset in Fig. 8b).

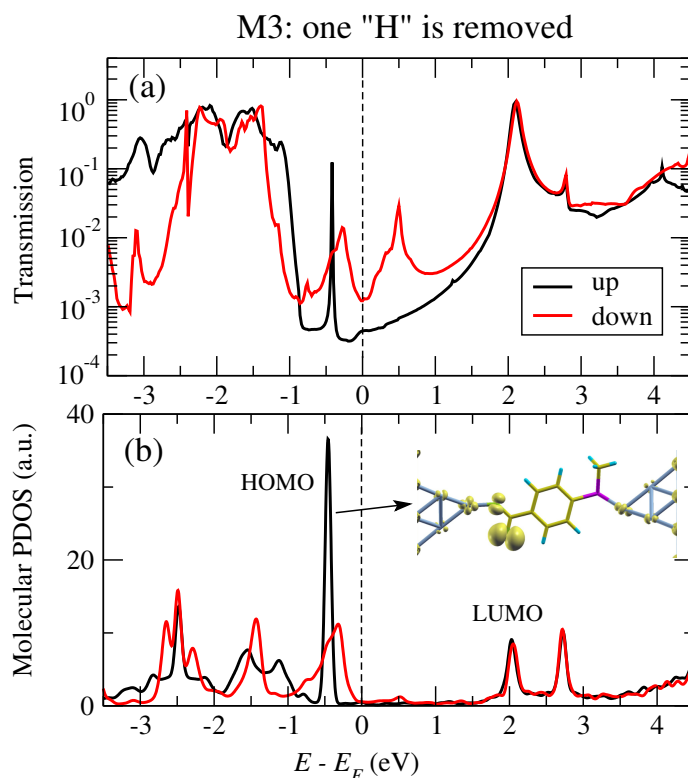


Figure 8. M3 molecular junction with COO^- -Ni contact, here one “H” atom is removed. Spin-resolved transmission function (a) and projected DOS on molecule (b). Spin up and down channels are plotted by black and red lines, respectively. Note that the zero of energy is at the Fermi level. Local DOS at the energy range of HOMO peak for spin up is plotted in the inset.

342 Appendix D: Spin-dependent $T(E)$ with the anti-parallel spin configuration

343 We present in Fig. 9 the spin-dependent transmission functions for the anti-parallel
 344 magnetic configuration of two Ni electrodes. Due to symmetry, spin up and spin down
 345 $T(E)$ superpose for symmetric junctions (M1, M2, M5 and M6) while they are slightly
 346 different for asymmetric cases (M3 and M4). The corresponding magnetoresistance
 347 values are summarized in Table. 2.

	M1	M2	M3	M4	M5	M6
MR (%)	35	10	30	38	92	142

Table 2. Calculated magnetoresistance, $\text{MR} = (G_P - G_{\text{AP}})/G_{\text{AP}} \times 100\%$, of six molecular junctions.

348 References

349 [1] Sanvito S 2011 *Chemical Society Reviews* **40** 3336–3355

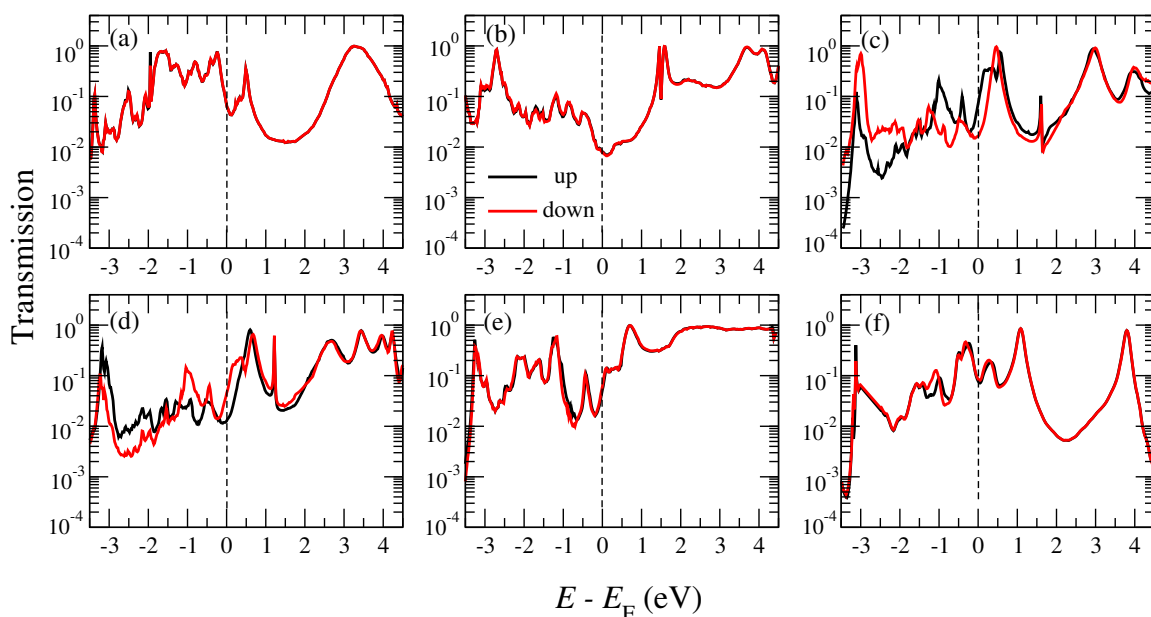


Figure 9. Spin-resolved zero-bias transmission functions (in logarithmic scale) with the anti-parallel magnetic alignment of two Ni electrodes for (a) M1, (b) M2, (c) M3, (d) M4, (e) M5 and (f) M6 molecular junctions. Spin up and down channels are plotted by black and red lines, respectively. Note that the zero of energy is at the Fermi level.

- 350 [2] Atodiressei N, Brede J, Lazić P, Caciuc V, Hoffmann G, Wiesendanger R and Blügel S 2010 *Phys.*
 351 *Rev. Lett.* **105**(6) 066601
- 352 [3] Barraud C, Seneor P, Mattana R, Fusil S, Bouzehouane K, Deranlot C, Graziosi P, Hueso L,
 353 Bergenti I, Dediu V *et al.* 2010 *Nature Physics* **6** 615
- 354 [4] Requist R, Baruselli P P, Smogunov A, Fabrizio M, Modesti S and Tosatti E 2016 *Nature*
 355 *nanotechnology* **11** 499
- 356 [5] Tang Y H and Lin C J 2015 *The Journal of Physical Chemistry C* **120** 692–696
- 357 [6] Smogunov A and Dappe Y J 2015 *Nano Letters* **15** 3552–3556
- 358 [7] Li D, Banerjee R, Mondal S, Maliyov I, Romanova M, Dappe Y J and Smogunov A 2019 *Phys.*
 359 *Rev. B* **99**(11) 115403
- 360 [8] Chen F, Li X, Hihath J, Huang Z and Tao N 2006 *Journal of the American Chemical Society* **128**
 361 15874–15881
- 362 [9] Ke S H, Baranger H U and Yang W 2004 *Journal of the American Chemical Society* **126** 15897–
 363 15904
- 364 [10] Venkataraman L, Klare J E, Tam I W, Nuckolls C, Hybertsen M S and Steigerwald M L 2006
 365 *Nano letters* **6** 458–462
- 366 [11] Li C, Pobelov I, Wandlowski T, Bagrets A, Arnold A and Evers F 2008 *Journal of the American*
 367 *Chemical Society* **130** 318–326
- 368 [12] Park Y S, Whalley A C, Kamenetska M, Steigerwald M L, Hybertsen M S, Nuckolls C and
 369 Venkataraman L 2007 *Journal of the American Chemical Society* **129** 15768–15769
- 370 [13] Meisner J S, Kamenetska M, Krikorian M, Steigerwald M L, Venkataraman L and Nuckolls C 2011
 371 *Nano letters* **11** 1575–1579
- 372 [14] Ahn S, Aradhya S V, Klausen R S, Capozzi B, Roy X, Steigerwald M L, Nuckolls C and
 373 Venkataraman L 2012 *Physical Chemistry Chemical Physics* **14** 13841–13845
- 374 [15] Farzadi R, Moghaddam H M and Farmanzadeh D 2018 *Chemical Physics Letters* **704** 37 – 44
- 375 [16] Xue Y and Ratner M A 2004 *Phys. Rev. B* **69**(8) 085403

- 376 [17] Obersteiner V, Egger D A and Zojer E 2015 *The Journal of Physical Chemistry C* **119** 21198–21208
- 377 [18] Kamiński W, Topolnicki R, Hapala P, Jelínek P and Kucharczyk R 2016 *Organic Electronics* **34**
- 378 254–261
- 379 [19] Venkataraman L, Park Y S, Whalley A C, Nuckolls C, Hybertsen M S and Steigerwald M L 2007
- 380 *Nano letters* **7** 502–506
- 381 [20] Tsukamoto S, Caciuc V, Atodiresei N and Blügel S 2012 *Phys. Rev. B* **85**(24) 245435
- 382 [21] Li D, Barreateau C, Kawahara S L, Lagoute J, Chacon C, Girard Y, Rousset S, Repain V and
- 383 Smogunov A 2016 *Phys. Rev. B* **93**(8) 085425
- 384 [22] Arnoux Q, Blouzon C, Li D, Dappe Y J, Smogunov A, Bonville P, Tortech L and Moussy J B
- 385 2019 *Phys. Rev. B* **99**(14) 144405
- 386 [23] Cakır D, Otálvaro D M and Brocks G 2014 *Physical Review B* **90** 245404
- 387 [24] Bairagi K, Bellec A, Repain V, Chacon C, Girard Y, Garreau Y, Lagoute J, Rousset S, Breitwieser
- 388 R, Hu Y C, Chao Y C, Pai W W, Li D, Smogunov A and Barreateau C 2015 *Phys. Rev. Lett.*
- 389 **114**(24) 247203
- 390 [25] Cinchetti M, Dediu V A and Hueso L E 2017 *Nature materials* **16** 507
- 391 [26] Zhang Z, Qiu S, yuan Miao Y, feng Ren J, kui Wang C and chao Hu G 2017 *Applied Surface*
- 392 *Science* **409** 60 – 64
- 393 [27] Qiu S, Zhang Z, yuan Miao Y, ping Zhang G, feng Ren J, kui Wang C and chao Hu G 2018 *Applied*
- 394 *Surface Science* **427** 416 – 420
- 395 [28] Emberly E G and Kirczenow G 2002 *Chemical Physics* **281** 311–324
- 396 [29] Waldron D, Haney P, Larade B, MacDonald A and Guo H 2006 *Phys. Rev. Lett.* **96**(16) 166804
- 397 [30] Rocha A R, Garcia-Suarez V M, Bailey S W, Lambert C J, Ferrer J and Sanvito S 2005 *Nature*
- 398 *materials* **4** 335
- 399 [31] Rakhmilevitch D, Sarkar S, Bitton O, Kronik L and Tal O 2016 *Nano letters* **16** 1741–1745
- 400 [32] Li D, Dappe Y J and Smogunov A 2016 *Phys. Rev. B* **93**(20) 201403(R)
- 401 [33] Giannozzi P, Baroni S, Bonini N, Calandra M, Car R, Cavazzoni C, Ceresoli D, Chiarotti G L,
- 402 Cococcioni M, Dabo I, Dal Corso A, de Gironcoli S, Fabris S, Fratesi G, Gebauer R, Gerstmann
- 403 U, Gougoussis C, Kokalj A, Lazzeri M, Martin-Samos L, Marzari N, Mauri F, Mazzarello R,
- 404 Paolini S, Pasquarello A, Paulatto L, Sbraccia C, Scandolo S, Sclauzero G, Seitsonen A P,
- 405 Smogunov A, Umari P and Wentzcovitch R M 2009 *Journal of physics. Condensed matter* **21**
- 406 395502
- 407 [34] Perdew J P, Burke K and Ernzerhof M 1996 *Phys. Rev. Lett.* **77**(18) 3865–3868
- 408 [35] Brandbyge M, Mozos J L, Ordejón P, Taylor J and Stokbro K 2002 *Phys. Rev. B* **65**(16) 165401
- 409 [36] Troullier N and Martins J L 1991 *Phys. Rev. B* **43**(3) 1993–2006
- 410 [37] Soler J M, Artacho E, Gale J D, García A, Junquera J, Ordejón P and Sánchez-Portal D 2002
- 411 *Journal of Physics: Condensed Matter* **14** 2745
- 412 [38] Lee S K, Ohto T, Yamada R and Tada H 2014 *Nano letters* **14** 5276–5280
- 413 [39] Quek S Y, Kamenetska M, Steigerwald M L, Choi H J, Louie S G, Hybertsen M S, Neaton J and
- 414 Venkataraman L 2009 *Nature nanotechnology* **4** 230
- 415 [40] Zotti L A, Kirchner T, Cuevas J C, Pauly F, Huhn T, Scheer E and Erbe A 2010 *small* **6** 1529–1535
- 416 [41] Kaliginedi V, V Rudnev A, Moreno-Garca P, Baghernejad M, Huang C, Hong W and Wandlowski
- 417 T 2014 *Phys. Chem. Chem. Phys.* **16**(43) 23529–23539
- 418 [42] Vardimon R, Klionsky M and Tal O 2015 *Nano Letters* **15** 3894–3898
- 419 [43] Leary E, Zotti L A, Miguel D, Mrquez I R, Palomino-Ruiz L, Cuerva J M, Rubio-Bollinger G,
- 420 Gonzlez M T and Agrait N 2018 *The Journal of Physical Chemistry C* **122** 3211–3218
- 421 [44] Inkpen M S, Liu Z F, Li H, Campos L M, Neaton J B and Venkataraman L 2019 *Nature chemistry*
- 422 1
- 423 [45] Sheng W, Li Z Y, Ning Z Y, Zhang Z H, Yang Z Q and Guo H 2009 *The Journal of Chemical*
- 424 *Physics* **131** 244712
- 425 [46] Strange M, Rostgaard C, Häkkinen H and Thygesen K S 2011 *Phys. Rev. B* **83**(11) 115108
- 426 [47] Rangel T, Ferretti A, Olevano V and Rignanese G M 2017 *Phys. Rev. B* **95**(11) 115137

- 427 [48] Elbing M, Ochs R, Koentopp M, Fischer M, von Hänisch C, Weigend F, Evers F, Weber H B and
428 Mayor M 2005 *Proceedings of the National Academy of Sciences* **102** 8815–8820
- 429 [49] Batra A, Darancet P, Chen Q, Meisner J S, Widawsky J R, Neaton J B, Nuckolls C and
430 Venkataraman L 2013 *Nano Letters* **13** 6233–6237
- 431 [50] Rivero P, García-Suárez V M, Pereñíguez D, Utt K, Yang Y, Bellaiche L, Park K, Ferrer J and
432 Barraza-Lopez S 2015 *Computational Materials Science* **98** 372–389